Chalcogenide Letters Vol. 18, No. 9, September 2021, p. 493 - 504

First-principles studies of the structural, elastic, vibrational, and thermodynamic properties of nonlinear chalcogenide $LiGaTe_2$ under pressure

M. Guenfoud[a,*], M. Hamouda[a], I. Arbaoui[b]
[a]*LDDI–Laboratory, Faculty of Science and Technology, University Ahmed Draia of Adrar, 01000, Algeria*
[b]*LESEM Laboratory, Oran1 University, Ahmed Ben Bella, 31000, Algeria*

First-principles calculations for the structural, elastic, thermal and vibrational properties of $LiGaTe_2$ under pressure up to 5GPa have been systematically investigated within the framework of the density functional theory. The lattices parameters found *a*, *c* and the bulk modulus *B* under zero pressure and zero temperature are close with the experimental data and the theoretical results. The analysis of the mechanical constants and the frequencies of the phonons found, confirms that the compound $LiGaTe_2$ is dynamically and mechanically stable up to 5GPa. The effect of pressure on elastic constants C_{ij}, bulk modulus *B*, Young's modulus *E*, Poisson ratio ν, shear modulus *G*, and compressibility *k* of $LiGaTe_2$ are also successfully obtained and discussed. In addition, the thermal properties of $LiGaTe_2$, such the heat capacity C_V and C_p, the grüneisen parameter γ and the thermal expansion coefficient α are predicted by the quasi-harmonic approximation (QHA).

(Received June 28, 2021 ; Accepted September 1, 2021)

Keywords: $LiGaTe_2$, LO-TO splitting, Elastic, Vibrational, Thermal properties

1. Introduction

Tellurium-based chalcopyrite ternary compounds have become a very studied group of materials in recent years due to their interesting optical characteristics such as a wide range of transparency in the infrared domain, high nonlinear sensitivity and birefringence [1-3]. One of this group of crystalline materials, $LiGaTe_2$ (LGT) is of great importance in nonlinear optics applications, due to its specific characteristics: a wide direct band gap [4], wide range of transparency [5] and high nonlinear susceptibility [6]. These settings make it twice as efficient as $AgGaAs_2$ for frequency conversion in the medium IR [7]. Many theoretical and experimental studies have been carried out to study this promising material. The growth of $LiGaTe_2$ has been reported by several methods [6-8]. Very recently, Grazhdannikov et al. [9] succeeded in growing large LGT crystals (up to 12 mm in size) by the Bridgman-Stockbarger technique in vertical version. The heat capacity of $LiGaTe_2$ chalcogenide monocrystalline disks was first measured by Drebushchak et al. [10] in a scanning mode of 180 to 460 K. A. Yelisseyev et al. [11] studied IR and Raman absorption spectra for $LiGaTe_2$ in the 50-350 cm^{-1} range. Elastic constants are essential physical quantities to describe the mechanical properties of materials.

These physical quantities can inform us about the structural stability of materials. Unfortunately, the study of these constants under pressure is rare [12]. Consequently, a systematic study of these properties (especially under pressure) is essential, especially if one wishes to use these materials in new applications. It can be noted that understanding the abnormal thermal expansion of the $LiGaTe_2$ crystal [13] requires a precise description of the phonon spectra. These phonon spectra are essential for predicting thermodynamic properties and are very useful in understanding the origin of these properties and their response to various thermodynamic conditions.Motivated by this, the vibrational and mechanical properties of $LiGaTe_2$ under different hydrostatic pressures are investigated as part of the first principles density functional perturbation theory. Dynamic stability was checked by examining the phonon spectra under different pressures.

* Corresponding author: sciencestech@yahoo.fr
https://doi.org/10.15251/CL.2021.189.493

In addition, thermal properties were determined using the Quasi-Harmonic Approximation (QHA) method [14-16]. These results should provide a valuable estimate for the theoretical and experimental research of chalcogenide $LiGaTe_2$.

The rest paper is processed as follows. The calculation method is introduced and described in the second section. In the third section, some results are exposed and discussed. Finally, a summary of our main results is presented at the end of this paper.

2. Computational methods

In present paper, all calculations were obtained by using VASP package [17-21] which is based on the density-functional theory [22, 23]. Exchange and correlations effects were treated by the generalized gradient approximation (GGA) with the Perdew-Burke-Ernzernhof parameterization (PBE) [23]. Moreover, a comparative analysis of DFT predictions on the curves dispersion of phonons was made with local density approximation (LDA) [24]. The valence states of the atoms of Li, Ga, and Te were taken as $2s^1$, $3d^{10}4s^2p^1$ and $5s^25p^4$, respectively. The cut-off energy was set to 650 eV, and the brillouin zone was sampled over 8 8 8 points by the monkhorst pack scheme [25]. The total energy change between 2 self-consistent steps was smaller than was obtaine10^{-8} eV/atom, and atomic relaxation was stopped when the Hellmann-Feynaman ionic forces fell below 10^{-3} eV/Å. The Calculations of the vibrational characteristics of the phonons were performed by the linear response approach as implemented in the PHONOPY code [26], in combination with VASP. A 2 × 2 × 2 supercell (64 atoms) developed from the primitive unit cell (08 atoms, six coordination layers) and a 2 × 2 × 2 k mesh were adopted to calculate the vibrational properties including the curves dispersion of phonons and the density of the states of the phonons, as well as the frequencies of the phonons.

3. Results and discussion

3.1. Structural properties

The ternary compound $LiGaTe_2$ generally crystallize in the centered tetragonal structure of chalcopyrite belonging to space group I$\bar{4}$2d (No.122) [27], with the Li, Ga and Te atoms belonging to the Wyckoff sites of 4a, 4b and 8d, respectively. The structural parameters are acquired by minimizing the total energy as a function of the unit cell volumes around the equilibrium volume V_0. The E-V results are fitted to the Birch-Murnaghan equation of state EOS [28], as showed in fig. 1

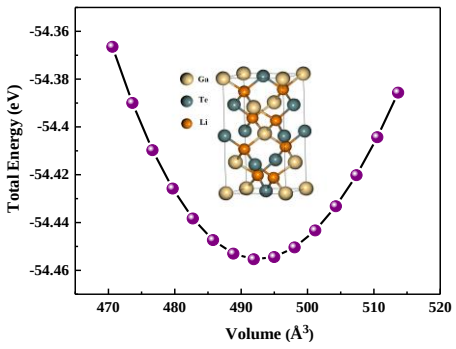

Fig. 1. The total energy per formula unit as function of volume for $LiGaTe_2$. The inset is the corresponding crystal structure.

The optimized lattice constant *a (c)* (in unit Å), tetragonal distortion (*c/a)*, cell volume *V*(Å^3), internal parameter *u* and bulk modulus *B* (GPa) for $LiGaTe_2$ are presented in table 1,

together with the available theoretical and experimental results. It can be seen that the optimized lattice constants of $LiGaTe_2$ are a = 6.401 and c = 12.008Å.

The lattice constants a or c are a little larger than those of experimental data [31, 32], due to the GGA overestimating the lattice constants slightly.

Table 1. The lattice constant a (c) (in unit Å), tetragonal distortion (c/a), cell volume V(Å^3), internal parameter u and bulk modulus B (GPa) for $LiGaTe_2$.

Method	*a*	*c*	*c/a*	*V*	*u*	*B*
Present work (VASP-GGA-PBE)	6.401	12.008	1.876	492.00	0.2643	26.770
Present work (VASP-LDA)	6.218	11.706	1.883	452.60	0.2608	32.092
WIEN2K-EV-GGA (Ref. [29])	6.433	11.873	–	–	0.2308	35.49
WIEN2K-GGA-PBE (Ref. [12])	6.381	12.027	1.885	491.54	0.2611	33.889
PWscf-LDA (Ref. [30])	6.211	11.690	–	–	0.2591	–
Exp. (Ref. [31])	6.329	11.682	1.85	468.0	0.2666	–
Exp. (Ref. [32])	6.338	11.704	–	470.1	–	–

Fig. 2.b shows the effect of pressure on the lattice constants up to 5 GPa. It is clearly seen that the optimized mesh parameters gradually decrease with increasing pressure. this indicates that $LiGaTe_2$ exhibits an anisotropic property when external pressure is applied. To show the anisotropic character more clearly, the reduced lattice constants are plotted in Fig. 1.a, where a_0 and c_0 are the lattice constants at pressure 0. We can observe that the (a / a_0) drops faster than the (c / c_0) with pressure, demonstrating that the chalcopyrite compound $LiGaTe_2$ is easily compressed in direction a.

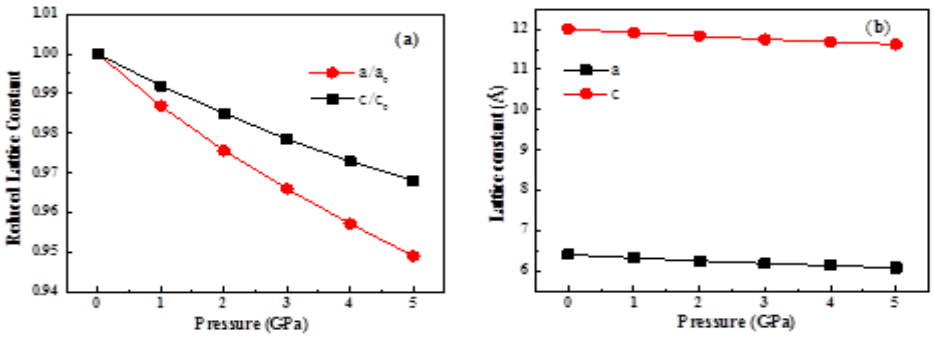

Fig. 2. (a) Reduced lattice constants, (b) calculated lattice constants for the $LiGaTe_2$ as a function of the hydrostatic pressure.

3.2. Elastic Properties

For chalcopyrite compounds, there are six independent components elastic stiffness constants due to the symmetry of the I42d space group, namely: C_{11}, C_{12}, C_{13}, C_{33}, C_{44} and C_{66}, respectively. The calculated values of the elastic constants were checked by Born elastic stability criteria [33], which for the tetragonal crystals are: $C_{11} > 0$, $C_{33} > 0$, $C_{44} > 0$, $C_{66} > 0$, $C_{11} > |C_{12}|$, $C_{11}C_{33} > C^2_{13}$ and $2C^2_{13} < C_{33}(C_{11} + C_{12})$. The elastic constants obtained are given in table 2. It can be seen that our calculated elastic constants satisfy all these conditions, which reflects the mechanic stability of $LiGaTe_2$.From Table 2, we can see that C_{11} has a smaller value than C_{33}, which means $LiGaTe_2$ is easily compressed along the a-axis with respect to the c-axis.

Table. 2 Elastic constants C_{ij} (in GPa) of $LiGaTe_2$ under pressure 0 Gpa.

Refs.	C_{11}	C_{12}	C_{13}	C_{33}	C_{44}	C_{66}
Present work (VASP-GGA-PBE)	38.6	17.6	22.8	39.7	18.9	14.1
Present work (VASP -LDA)	44.1	22.3	28.3	46.4	20.1	14.4
Ref. [30]	44.2	21.6	28.2	46.6	20.0	14.5
Ref. [12]	56	29.2	32	45.4	40.7	39.1

With the elastic constants found, the polycrystalline elastic properties such as the bulk modulus (*B*), Young's modulus (*E*), shear modulus (*G*) and Poisson's ratio (ν), were calculated by using the Voigt–Reuss–Hill (VRH) averaging scheme [34-37]. The theoretical values for polycrystalline elastic properties are listed in table 3.

Table. 3 Calculated bulk modulus B (GPa), shear modulus G (GPa), Young modulus E (GPa), Poisson's ratio ν and the linear compressibilities κ_a (GPa^{-1}), κ_c (GPa^{-1}) along the a- and c- axis respectively of $LiGaTe_2$ under pressure 0 GPa.

Refs.	*B*	*G*	*E*	*v*	κ_a	κ_c
Present work (VASP-GGA-PBE)	26.926	13 .099	33.814	0.2907	0.0142	0.009
Present work (VASP -LDA)	32.299	13.670	35.940	0.315	0.0122	0.0066
Ref. [30]	31.9	–	–	–	0.0125	0.0063

The calculated bulk modulus *B* of the $LiGaTe_2$ at 0 K and 0 GPa is 26.926 GPa, which is in agreement with the result of 26.77 GPa obtained from fitting Birch-Murnaghan (EOS).

The linear compressibility κ_a and κ_c along the *a*-axis and *c*-axis respectively for the tetragonal structure can be deduced from the following equations [38]:

$$\kappa_a = -\frac{1}{a}\frac{\partial a}{\partial p} = \frac{C_{33} - C_{13}}{C_{33}(C_{11} + C_{12}) - 2C_{13}^2} \quad (1)$$

$$\kappa_c = -\frac{1}{a}\frac{\partial c}{\partial p} = \frac{C_{11} + C_{12} - 2C_{13}}{C_{33}(C_{11} + C_{12}) - 2C_{13}^2} \quad (2)$$

The elastic anisotropy of a crystal of tetragonal structure can be defined as the ratio of the axial compressibilities, κ_a/κ_c. The κ_a/κ_c ratio is 1.58 indicating that the a- axis is more compressible than the c- axis. This is in accordance with the C_{33}/C_{11} ratio greater than 1. The Poisson's ratio ν makes it possible to predict the stability of the crystal under the effect of a shear. The critical value of ν is 0.26, which falls between brittle and ductile behavior. If this value is smaller than 0.26, the material is said to be brittle, otherwise it is ductile [39]. We can clearly see that $LiGaTe_2$ is ductile in nature, which is consistent with the previous discussion. The calculated pressure dependences of elastic constants, *G*/*B* ratio, Poisson's ratio *v* and elastic moduli, for the chalcopyrite-type $LiGaTe_2$ are also plotted in Fig.3. Figure 3.a shows that C_{11}, C_{12}, C_{13}, and C_{33} vary significantly with applied pressure, while C_{44} and C_{66} vary slightly with applied pressure. In addition, the C_{11} is more sensitive to pressure than the C_{44}. This is because C_{11} describes elasticity in length while C_{44} relates to elasticity in shape. Therefore, the longitudinal deformation changes the value of C_{11}, while the transverse deformation causes a change in shape.

From figure 3-c, the calculated compression modulus *B* increases monotonically with increasing pressure, so this indicates that $LiGaTe_2$ becomes more and more difficult to compress

with increasing pressure, while that the variation of shear modulus *G* and Young's modulus *E* is almost invariant with increasing pressure. The high / low value of the G / B ratio is related to ductility / brittleness. The critical value between ductile and brittle materials is practically fixed at 0.5. The calculated G / B values for the LGT compound are less than 0.5, which implies ductile behavior.

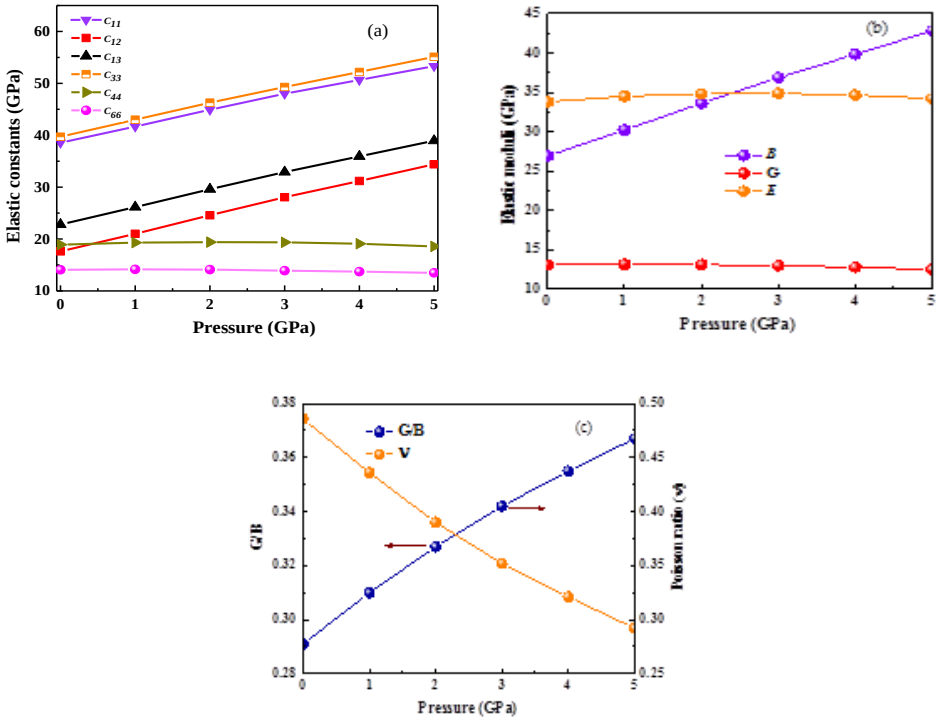

Fig. 3. (a) Elastic constants, (b) elastic moduli, (c) G/B ratio and Poisson's ratio v, for the chalcopyrite-type $LiGaTe_2$ as a function of the hydrostatic pressure.

With the elastic constants calculated above, it is possible to obtain the direction dependent of Young's modulus (*E*) and bulk modulus (*β*). Their formulas for tetragonal crystals are [40]:

$$\frac{1}{E} = S_{11}(l_1^4 + +l_2^4) + (2S_{13} + S_{44})(l_1^2 l_3^2 + l_2^2 l_3^2) + S_{33} l_3^4 + (2S_{12} + S_{66}) l_1^2 l_2^2 \quad (3)$$

$$\frac{1}{B} = (S_{11} + S_{12} + S_{13})(l_1^2 + l_2^2) + (2S_{13} + S_{33}) l_3^2 \quad (4)$$

For isotropic systems, the curved surface is spherical and the deviation from the spherical shape reflects the extent of elastic anisotropy. Fig.4 shows that the representations of the surfaces (3D) of the direction-dependent Young's modulus for LGT at 0 and 5 GPa are very similare, and their surface shape is no longer spherical, which implies a serious anisotropy. From fig. 4(b-d) we can see that the Young's modulus has a very high anisotropy along the 100 and 010 planes. To better see the elastic anisotropy, the linear compressibilities are plotted in Fig. 5. It can be seen that the direction-dependent linear compressibility in the (001) plane is almost isotropic, while in the (100) and (010) planes is not. The values in the (001) plane are greater than those of the (100) and (010) planes at 0 (a, b) and 5 GPa (c, d).

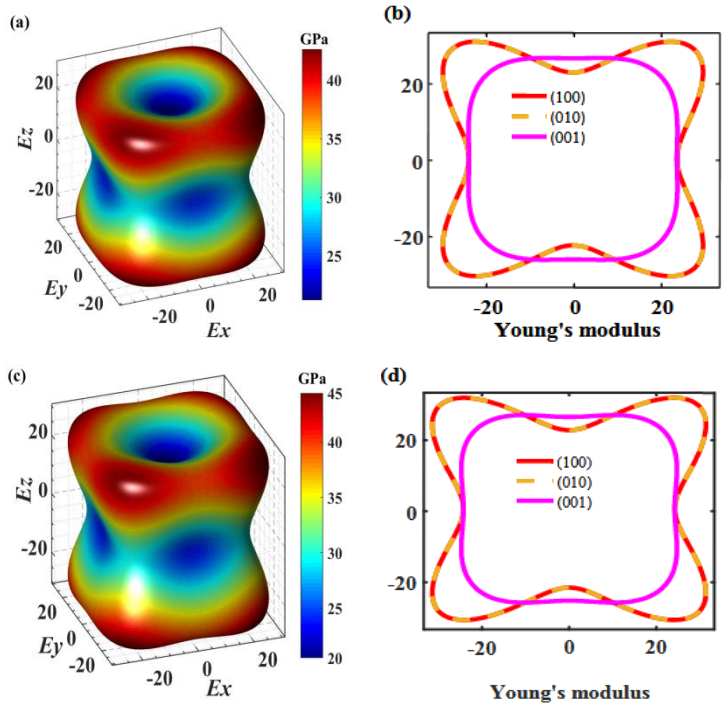

Fig. 4. Direction-dependent of Young's modulus (GPa) and its plane projections for $LiGaTe_2$ at 0 (a,b) and 5GPa (c,d).

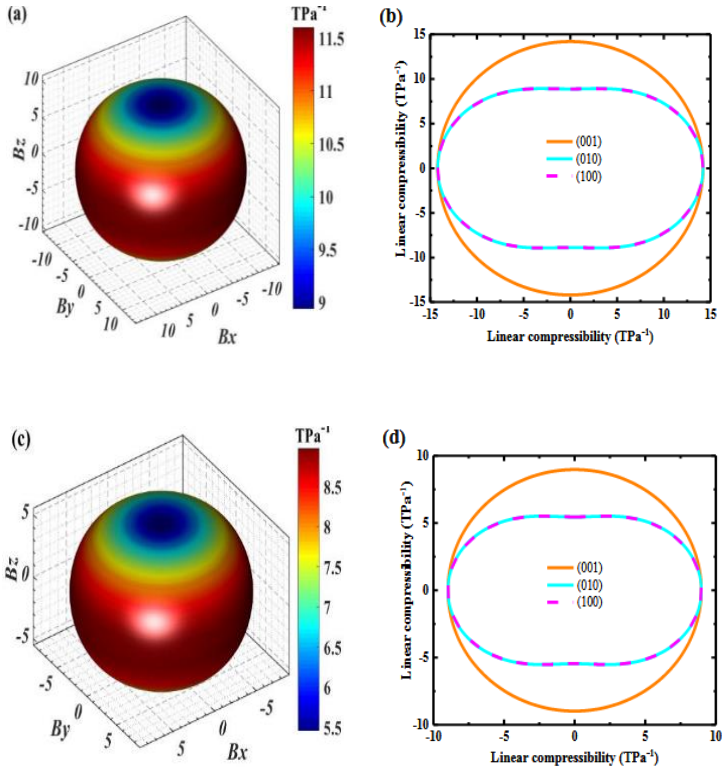

Fig. 5. Direction-dependent of linear compressibility (TPa^{-1}) and its plane projections for $LiGaTe_2$ at 0 (a,b) and 5GPa (c,d).

3.3. Vibrational Properties

Group-theorical analysis for space group I-42d predicts that the irreducible representation of the acoustic and optical vibrational modes at the center Γ of the Brillouin zone can be represented as [41]:

$$\Gamma_{aco} = B_2 + E \quad (5)$$

$$\Gamma_{opt} = A_1 + 2A_2 + 3B_1 + 3B_2 + 6E \quad (6)$$

Since the primitive cell of chalcopyrite structure contains eight atoms, the phonon dispersion curve at the center of ZB has twenty-four branches: 3 acoustic branches and 21 optical branches. According to the selection rules of infra-red (IR) absorption and Raman scattering, among these 24 modes, all modes, except A_2 mode, are Raman active, and only B_2 and E modes are IR active. Furthermore, the A_2 vibrational mode is called silent vibrational mode. There are totally thirteen Raman-active (R) modes, nine IR-active (IR) modes and two silent modes for $LiGaTe_2$ compound. Furthermore, B_2 and E are polar Raman active modes comprising longitudinal optical (LO) and transverse optical (TO) modes.

The phonon dispersion curve of $LiGaTe_2$ compound along the high symmetry points in the (ZB) and the corresponding phonon density of states are shown in Fig.6. It can be seen clearly that there are no soft modes found at any wave vectors above in the phonon dispersion curve, implying that this structure is dynamically stable at 0GPa. We can distinguish relatively three regions at point Γ: The low frequency zone around 0-150 cm^{-1}, come overall from the vibration of Te atoms owing to its heavy atomic weight, a medium frequency zone between 150 and 250 cm^{-1}, results from the vibration of the three constituent atoms, especially the Ga and Te atoms, and high frequency zone above 300 cm^{-1} are mainly from the vibration of Li. The overlap of the bands of certain optical and acoustic modes in fig.6 makes the transfer of energy between these modes easy.

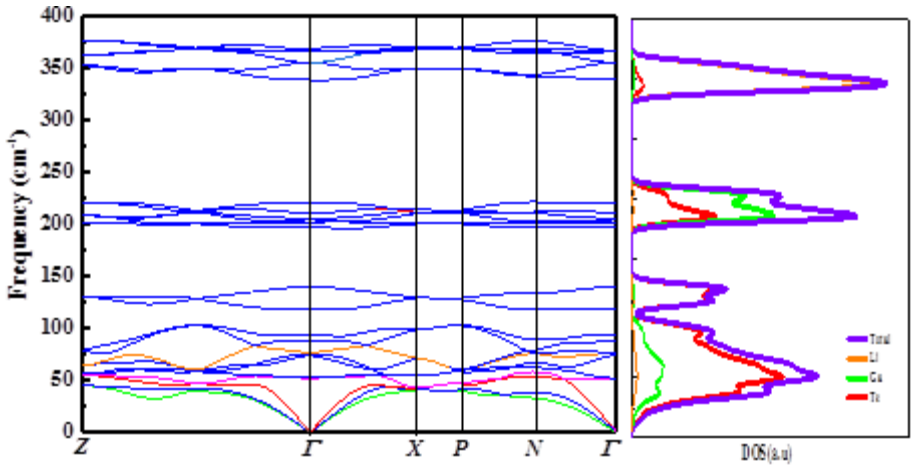

Fig. 6. Phonon dispersion curve along with the phonon density of states (DOS) of $LiGaTe_2$ at 0GPa.

Table 4 lists the optical vibrations modes and their corresponding frequencies of $LiGaTe_2$ compound calculated at Γ point in the Brillouin zone as well as the Raman [42], infrared [42] data and other calculations [13, 30]. Our calculated frequencies are very close to the theoretical data in Ref. [13] and Raman data from Isaenko et al. [42]. Unfortunately, some modes of vibration have not been observed in infrared and Raman measurements [42]. A_1 mode is unique. In addition it is totally symmetrical. It is associated with the vibration of the atom Te. According to our calculations for this mode, this value is estimated at 140 cm^{-1} for the LDA and 137 cm^{-1} for the GGA, which are identical to the theoretical values, reported by [30] and [13], and approach the Raman data reported by [42].

Table 4. Phonon frequencies (THz) at zone center (Γ point) of $LiGaTe_2$.

Mode	Theory Present			Theory			Experiment [42]	
	LDA	GGA-PBE		Ref [30]	Ref [13] 303 K		Raman	IR
	118	115		119	118		120	–
A_1	140	137		140	140		142	–
A_2	94	92		97	94		97	–
	366	342		342	313		–	–
B_1	205	199		204	192		198	–
	88	86		86	84		88	–
	355/355	327/318		336/327	313		–/321	–
B_2 (LO/TO)	211/205	216/207		210/195	187		–/196	215/202
	75/74	73/73		77/74	75		–	–
	369/346	350/342		358/343	300		360/340	360/340
E (LO/TO)	339/339	337/336		339/339	311		325	–
	221/211	206/201		222/212	208		221/211	–
	205/204	197/192		203/200	199		–	–
	77/77	77/74		78/77	79		76	–
	52/52	52/52		45/45	54		49/39	–

It should be noted that the A_2 symmetry vibration mode is inactive according to the group theory and the selection rules for infrared (IR) and Raman absorption for ideal crystals with chalcopyrite lattice. But, the measurements of the Raman spectra according to [42] contain the A_2 mode. This appearance of the A_2 mode is often observed, for chalcopyrite materials of defective structure which generates an additional contribution of phonons causing the A_2 mode to appear.

3.4. Thermodynamic properties

Within the framework of the quasi-harmonic method (QHA), and from the curves of dispersion of the phonons and density of state of the phonons, the thermal properties such as the contribution of the phonons to the free energy of Helmholtz ΔF and the specific heat at constant volume C_V, at temperature T, are obtained immediately.

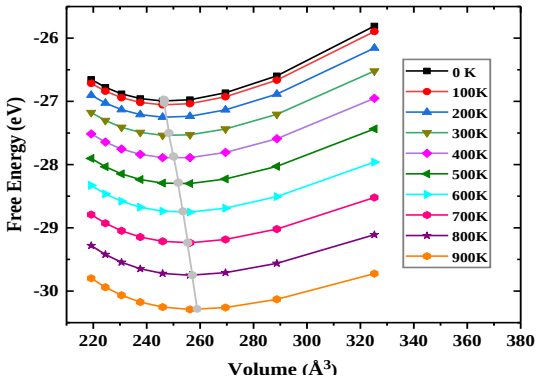

Fig. 7. Helmholtz free energy as a function of the lattice volume from 0 to 900 K. Solid lines are F-V fitting curves according to the Birch-Murnaghan equation of state EOS. The local minimum of each free energy curve is indicated by a grey line.

Figure 7 shows the variation of Helmholtz free energy as a function of volume from 0 to 900 K. The minimum energy points are connected by a gray line in Figure 7. As shown in this figure, the volume increases with increasing temperature; therefore, the equilibrium volume changes at each given temperature.

The Grüneisen parameters can give good information on the anharmonic interactions of a crystal. In general, it can be deduced from the relation between phonon frequency and volume change as below [43] :

$$\gamma_{(\lambda,q)} = \frac{-V}{\omega_{\lambda,q}} \frac{\partial \omega_{\lambda,q}}{\partial V} \tag{7}$$

Usually, a large value of | γ | means that it could have a strong phonon-phonon anharmonic scattering. The mode grüneisen parameter as functions of temperature and frequencies are plotted in fig. 8. From figure 8.a we can clearly see that $LiGaTe_2$ exhibits very low grüneisen parameters, indicating that it has low anharmonicity. Under 90 cm^{-1}, $LiGaTe_2$ exhibits many negative gruunisen mode parameters, which indicate that the corresponding phonon frequencies will increase as the volume increases.

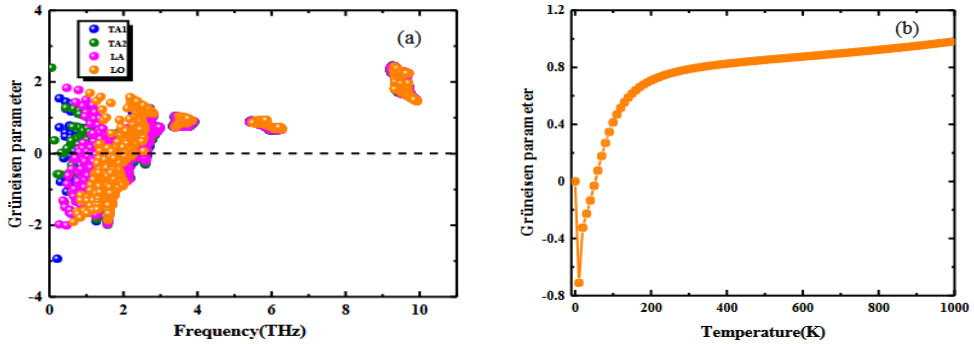

Fig. 8. Grüneisen parameters as a function of :(a) the frequency, (b) temperature, for $LiGaTe_2$.

At low temperature, since only low frequency phonons are excited, the average grüneisen parameters could be negative, as shown in fig. 7. Such a negative parameter is common in chalcopyrite type chalcogenides [44]. The most negative grüneisen parameters can be observed in the low frequency region, corresponding to the acoustic modes. According to the quasi-harmonic approximation (QHA), the variation of the grüneisen mode parameter contributes strongly to thermal expansion. We therefore used the frequency dependence of this parameter in the calculation of thermal expansion.

In the QHA approximation, the volume thermal expansion coefficient is defined by the following expression [45]:

$$\alpha_V = \frac{1}{V}\left(\frac{\partial V}{\partial T}\right)_P = \frac{1}{B}\left(\frac{\partial P}{\partial T}\right)_V \tag{8}$$

Fig.9 shows the thermal expansion coefficient as functions of temperature. It is seen that for $LiGaTe_2$, the coefficient of expansion decreases rapidly with temperature from 0 K, reaching its most negative value slightly below 50 K, then increases sharply.

This decrease occurring in the first 50 K is due to the increasing contribution of the optical modes of the phonons with temperature. The most negative value is about -5 $\times 10^{-6}$/K at around 40K. According to V. V. Atuchin et al [13], the negative thermal expansion of LGT along the c axis can be attributed to the rotation of the tetrahedra ($GaTe_4$), caused by the contribution of the B_2 vibration modes.

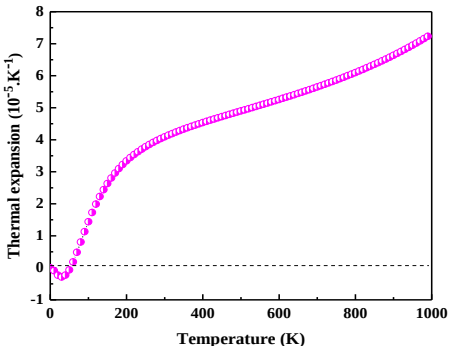

Fig. 9. The volume thermal expansion coefficient as a function of the temperature for $LiGaTe_2$.

The calculated heat capacity C_V of $LiGaTe_2$ as a function of T is shown in Fig.10. In the high temperature range, the heat capacity C_V reaches maximum values and approaches the classical asymptotic limit of *Dulong–Petit* (3*nkB*=200 J/mol K) [46]. At room temperature, the value of C_V is 170.27 J/mol K.

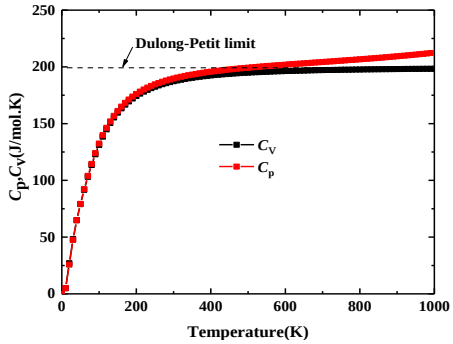

Fig. 10. Calculated specific heat as a function of the temperature for $LiGaTe_2$.

4. Conclusions

Thus, in this paper, the structural, elastic, dynamical, and thermodynamic properties of $LiGaTe_2$ under pressures were investigated using the density functional theory within a local density and generalized gradient approximations. The results showed that the pressure has a strong impact on the lattice parameters and the elastic properties of the $LiGaTe_2$. The calculated lattice parameter and bulk modulus agree well with the experimental data and the theoretical results available. The calculated elastic constants showed that this compound is mechanically stable. The vibrational properties of $LiGaTe_2$ have been calculated through the linear-response approach. All the infrared-active and Raman-active modes (including LO-TO splitting) are identified and compared with available experimental data and previous theoretical calculations. In the phonon dispersion curves, there are no soft modes along the Brillouin zone (BZ). Which confirms the dynamic stability of $LiGaTe_2$ under zero pressure and zero temperature.

The Heat capacity at constant volume C_V and constant pressure C_p are also been obtained by using the quasi-harmonic method. Finally, we found that the compound $LiGaTe_2$ has negative thermal expansion along the c axis which was attributed according to V. V. Atuchin et al [13], to the rotation of the tetrahedra ($GaTe_4$), caused by the contribution of the B_2 vibration modes.

To the best of our knowledge, most of the investigated parameters are reported for the first time and hoped to stimulate the succeeding studies and offer practical information for the future experiments.

Acknowledgments

The authors would like to extend their gratitude to the General Direction of Scientific Research and Technological Development (DGRSDT)-MESRS.

References

[1] I. Chung, M. G. Kanatzidis, Chemistry of Materials **26**(1), 849 (2014).
[2] S. Wang, H. Ruan, G. Liu, G. Zhang, Q. Shi, J. Cryst. Growth **362**, 271 (2013).
[3] L. Bai, Z. S. Lin, Z. Z. Wang, and C. T. Chen, J. Appl. Phys. **103**, 083111 (2008).
[4] J. J. Zondy, F. Bielsa, A. Douillet, L. Hilico, O. Acef, V. Petrov, A. Yelisseyev, L. Isaenko, P. Krinitsin, Opt. Lett. **12**, 1722 (2007).
[5] L. I. Isaenko, A. P. Yelisseyev, Semiconductor Science and Technology **31**(12), 123001 (2016).
[6] V. Petrov, L. Isaenko, A. Yelisseyev, P. Krinitsin, V. Vedenyapin, A. Merkulov, J. J.Zondy, J. Non cryst. Solids **352**, 2434 (2006).
[7] L. Isaenko, I. Vasilyeva, A. Merkulov, A. Yelisseyev, S. Lobanov, J. Cryst. Growth **275**, 1 (2005).
[8] E. Tupitsyn, P. Bhattacharya, E. Rowe, L. Matei, Y. Cui, V. Buliga, M. Groza,B. Wiggins, J. Cryst. Growth **393**, 23 (2014).
[9] S. A. Grazhdannikov, P. G. Krinitsyn, A. F. Kurus, L. I. Isaenko, A. P. Yelisseyev M. S. Molokeev, Materials Science in Semiconductor Processing **72**, 52 (2017).
[10] V. Drebushchak, L. Isaenko, S. Lobanov, P. Krinitsin, S. Grazhdannikov, Journal of Thermal Analysis and Calorimetry **129**(1), 103 (2017).
[11] A. Yelisseyev, P. Krinitsin, L. Isaenko, S. Grazhdannikov, Optical Materials **42**, 276 (2015).
[12] M. Bendjemai, H. Bouafia, B. Sahli, A. Dorbane, Ş. Uğur, G. Uğur, S. Mokrane, Physica B Physics of Condensed Matter **599**, 412463 (2020).
[13] V. V. Atuchin, F. Liang, S. Grazhdannikov, L. I. Isaenko, P. G. Krinitsin, M. S. Molokeev, I. P. Prosvirin, Xingxing Jiang, Zheshuai Lin, RSC Adv. **8**, 9946 (2018).
[14] N. S. Abraham, M. R Shirts, Crystal Growth Design **19**(12), 6911 (2019).
[15] A. Kuwabara, T. Tohei, T. Yamamoto, I. Tanaka, Phys. Rev. B **71**, 064301 (2005).
[16] T. Tohei, H.-S. Lee, Y. Ikuhara, Mater. Trans. **56**, 1452 (2015).
[17] G. Kresse, J. Furthmuller, Phys. Rev. B **54**, 11169 (1996).
[18] G. Kresse, J. Furthmuller, Comput. Mater. Sci. **615**, (1996).
[19] G. Kresse, D/ Joubert, Phys. Rev. B **59**, 1758 (1999).
[20] J. Hafner, Computer physics communications **177**, 6 (2017).
[21] K. Burke, J. Chem. Phys. **136**, 150901 (2012).
[22] W. Kohn, L. J. Sham, Phys. Rev. **140**, A1133 (1965).
[23] J. P. Perdew, K. Burke, M. Ernzerhof, Phys. Rev. Lett. **77**, 3865(1996).
[24] D. M.Ceperley, B. J. Alder, Phys. Rev. Lett. **45**, 566 (1980).
[25] H. J. Monkhorst, J D Pack Phys. Rev. B **13**, 5188 (1976).
[26] A. Togo, F. Oba, I. Tanaka, Phys. Rev. B **78**, 134106 (2008).
[27] W. Hönle, G. Kühn, H. Z. Neumann. Anorg. Allg. Chem. **150**, 532 (1986).
[28] F. Birch, Phys. Rev. **71**, 809 (1947).
[29] A. Khan, M. Sajjad, G. Murtaza, A. Laref, Zeitschrift für Naturforschung A **73**(7), 645 (2018).
[30] A. V. Kosobutsky, Yu. M, Basalaev, A. S. Poplavnoi Phys. Status Solidi. B **246**, 364 (2009).
[31] A. Yelisseyev, P. Krinitsin, L. Isaenko, S. Grazhdannikov, Optical Materials **42**, 276 (2015).
[32] L. Isaenko, A. Yelisseyev, S. Lobanov, A. Titov, V. Petrov, J.-J. Zondy, P.Krinitsin, A. Merkulov V. Vedenyapin, J. Smirnova, Cryst. Res. Technol. **38**, 379 (2003).
[33] M. Born,K.Huang, Dynamical Theory of Crystal Lattices (Oxford: Clarendon) (1954).
[34] W. Voigt, Lehrbuch der Kristallphysik, Taubner, Leipzig, (1928).
[35] A. Reuss, Z. Angew, Math. Mech. **9**, 49 (1929).
[36] R. Hill, Proc. Phys. Soc. A **65**, 350 (1952).

[37] G. Simmons, H. Wang, MIT Press, Cambridge, MA, (1971).
[38] S. Tomar, R. Gautam, C. Negi, S. Gupta, S. Bhardwaj, A. Verma, Chalcogenide Letters **16**(1), 1 (2019).
[39] S. Daoud, N. Bioud, N. Bouarissa, Materials Science in Semiconductor Processing. **31**, 124 (2015).
[40] J. F. Nye, Physical Properties of Crystals, Oxford university press (1985).
[41] Y. Yu, Y. H. Shen, J. Deng, X. L. Zheng, G. D. Zhao, Chalcogenide Letters **14**(10), 447 (2017).
[42] L. Isaenko, P. Krinitsin, V. Vedenyapin, A. Yelisseyev, A. Merkulov, J.-J. Zondy, V. Petrov, Growth Des. **5**, 1325 (2005).
[43] K. Brugger, Phys. Rev. **137**, A1826 (1965).
[44] W. Paszkowicz, R. Minikayev, P. Piszora, D. Trots, M. Knapp, T. Wojciechowski, R. Bacewicz, Applied Physics. A **116**(2), 767 (2014).
[45] Y. Yu, X. G. Kong, Y. H. Shen, J. Deng, Chalcogenide Letters. **16**(11), 513 (2019).
[46] D. Bolmatov, D. Zavyalov, M. Zhernenkov, E. T. Musaev, Y. Q. Cai, Annals of Physics **363**, 221(2015).